5-2023

# The Terroir of Swiss Cheese: A Temporal and Geomorphological Investigation of the Martian CO2 Sublimation Pits

Racine D. Cleveland
*University of Arkansas-Fayetteville*

## Citation

The Terroir of Swiss Cheese: A Temporal and Geomorphological Investigation of the Martian $CO_2$ Sublimation Pits


A thesis submitted in partial fulfillment of
the requirements for the degree of
Master of Science in Geography


by


Racine D. Cleveland
Oklahoma State University
Bachelor of Science in Geography, 2019


May 2023
University of Arkansas


Thesis is approved for recommendation to the Graduate Council.


_____
Jason A. Tullis, Ph.D.
Committee Chair


_____
Vincent F. Chevier, Ph.D.
Committee Member


_____
Jack D. Cothren, Ph.D.
Committee Member

**Abstract**

Observations by NASA Mars Global Surveyor showed evidence of rough topography on the South Pole of Mars. The topography is the result of $CO_2$ sublimation processes that occur through the changing seasons on the red planet. These sublimation areas are known to scientists as Swiss Cheese Features (SCF). SCF are erosional degradation pits that have been studied for over two decades. Studies show that these SCF increase in area over time, but these values are collected by hand on a per feature basis. Models for the pit evolution have also played a part in understanding these SCF. This work is time-intensive and can only produce results from relatively small selections of data. Current research lacks the ability to complete image pit object-based and multi-image measurements as well as simultaneously estimate areal statistics. This research investigated the use of object-based image analysis (OBIA) techniques on sublimation pits at high spatial resolution over large temporal domains. This was done using images acquired through the High-Resolution Imager and Science Experiment (HiRISE) onboard the Mars Reconnaissance Orbiter (MRO). The approach was tested on selected pits and compared to previous work for stand-alone growth rates. The results of this investigation increase both our capacity to effectively study the $CO_2$ pits as well as our knowledge of pit evolution as a factor of time with implications to understand the $CO_2$ cycle on the Martian South Pole.

**Acknowledgements**

**Dedication**

This thesis is dedicated to my father, David Cleveland. You set me up for success at a young age by encouraging me to look toward the stars. Your constant love and support are something that I have been blessed with ten times over. I cannot thank God enough for letting me have you as my role model. I love you to the moon and back, Dad.

**Table of Contents**

# List of Figures

**List of Tables**

**Introduction**

Remote sensing is a gateway to creating a tangible experience of other worlds. Having images available to the public brings to society the vision of space exploration. However, these images hold more than that because they are data repositories waiting to be analyzed. The start of remote sensing image processing began with pixel-based approaches and hand measurements for the importance of agricultural and ecosystem conservation management (Blaschke, 2010). Pixel-based approaches utilize the spatial differences in a given area, and where discrepancies occur, sub-pixel analysis can be applied (Hossain & Chen, 2019). Over the last two decades satellite observation has been accompanied with increased image quality and quantity. There is a great need for understanding land processes and change across a variety of sciences and applications, and the technology has often focused on vegetation for agricultural and ecosystem services. Throughout the development of these Earth-focused applications, per-pixel imaging has often leveraged nadir image, especially given that higher resolution images have issues when captured off-nadir (Im et. al, 2008). Issues also arise when pixel are of similar spectral variables, such as ice on the polar regions of Mars, sand dunes, or mercury cratering. Given limitations on the orbital approaches used for planetary remote sensing, there is a need for faster and more accurate image analysis for off-nadir images.

In 1979, Kieffer et al. wrote about the Viking infrared thermal mapper data of the Martian residual cap on the South Pole. An active climate was indicated by the observed frost and axial tilt of 24.4° thus creating seasons comparable to those on Earth. Both the north and the south poles of Mars hold layered deposits of water ($H_2O$) ice, dust, and $CO_2$ ice. Where they differ is in the residual summer caps of frost. Thomas et al. (2000) notes that the North Pole sublimates the entire $CO_2$ top layer leaving behind an $H_2O$ rich residual cap, while the South Pole only partially

1

sublimates its $CO_2$ leaving behind a $CO_2$-rich residual cap. The sublimation accounts for roughly a quarter of the $CO_2$ in the planet's atmosphere (Thomas et al., 2000). Organization of clouds in the Martian winters creates an accumulation of $CO_2$ frost on the surface of the planet. This accumulation is kept in a season cap (Neumann et al., 2003). Neumann et al. (2003) utilized Mars Orbiter Laser Altimeter (MOLA) data to look at the cloud heights and seasonal patterns over the poles. They found that the $CO_2$ clouds are produced at a lower atmosphere and are less stable. This brings the need for continued observation to determine the structure of the winter precipitation features (ex. snowflakes, hail, or deposition). There is a great need for processing techniques that can support multi-entity identification in the planetary science community.

Originally deemed "geographic object-based image analysis" (GEOBIA) due to its genesis is the 1960's with aerial photography, this technique utilized geometric attributes such as texture and pixel-proximity for photo evaluation. Due to its later uses in the medical and biological fields, the term was shortened to "object-based image analysis" (OBIA) from GEOBIA. A 1965 paper explained image analysis as studying the photos for significance of contextual information such as homogeneity (which is the ability of something to be the same as its next object), size, shape, or patterns (Colwell 1965). Colwell went on to play an integral part in the first Landsat mission to send a satellite in orbit of the Earth for imagery purposes. The 1980s-1990s experienced advances in analyzing big spatial data preserves. What began with agricultural uses for identifying land types and land use, now has evolved into city planning, topological classification, and many other applications. OBIA has been presented as a multi-step semi-automated process that will create a detection procedure that works more similarly to how the human brain sorts and categorizes objects seen through a person's eyes (Im et al. 2008). Pixel-based operations used in the past only utilize the spectral information from a given image regardless of the individual objects in the

images. The previous approaches lack the ability to analyze higher spatial resolution imagery due to an inability to correctly interpret large areas of heterogeneity between close pixels, also known in the remote sensing world as the 'salt and pepper' effect. Segmentation is the operation used to change the image from a per-pixel source image to distinct objects by dividing the image into smaller segments. OBIA combines these two approaches to create a well-rounded analysis of the image objects of interest by collecting spectral, spatial, and contextual information.

Prior work using OBIA in planetary science has proven successful, even in small strides. For example, Vamshi et. al. (2016) used a manually derived eCognition ruleset on both a panchromatic image and a digital terrain model (DTM), and the DTM won out as the more reliable option for producing meaningful objects. A ruleset is the term used for the workflow or specific set of tools run in a specific order. The unitless term, scale parameter, used by eCognition, determines the size of the object. Their minimum was 6 and max was 6300. After objects were selected, they were classified based on their circularity. The researchers wanted the circularity scale parameter (SP) value to be > 6.5. They also used the slope created from the DTM. Once they classified the large craters, they changed the SP to be smaller for the unclassified merged region and ran the MRS again. The steps were then performed in a loop until all craters were classified. They found a good correlation between the hand-measured diameters and the manually measured diameters. They believe the margin of error can be attributed to erosional degradation of slopes over time, and the non-circular forms of objects.

Emran et. al (2016) used OBIA to locate sand dunes at Hargraves Crater on Mars. The area surveyed was roughly 70 km$^2$ of sand dune distribution. This research created digital elevation models in conjunction with panchromatic images, similar to Vimshi et al. (2016), thus providing calibration and consistent projection through the images. The SP used was 40 with a shape of 0.6

and a compactness level of 0.5. These unitless parameters can be handpicked and manipulated based on the outcome of the tool once it has been executed. Their accuracy was tested against the Mars Global Digital Dune Database where they received a 91% overall success rate with the ruleset created. With the success of this study, the authors suggest this ruleset can be used against all areas with barchan dune fields on the surface of Mars.

OBIA has been used for volcanic geomorphology which can be translated to volcanoes on Mars and Venus, perhaps even IO. In Pedersen and Grosse (2013), a ruleset was created to evaluate the success of OBIA on volcano geomorphometry mapping. Segmentation of the volcanic slopes provided delimitations of subglacial edifices. The researchers speculate that further analysis could be done to determine the different areas of edifice flank and lava flow cap areas. This would allow for systematic classification of the different eruptions of volcanoes.

**Research Objectives**

This study aims to investigate the use of OBIA on Martian sublimation pits at high spatial resolution over temporal domains on Mars with the following questions:

1.    *Can OBIA be used to be accelerate image-object processes for planetary images?*

2.    *How does the surface area of the pits change over time?*

**Study Area**
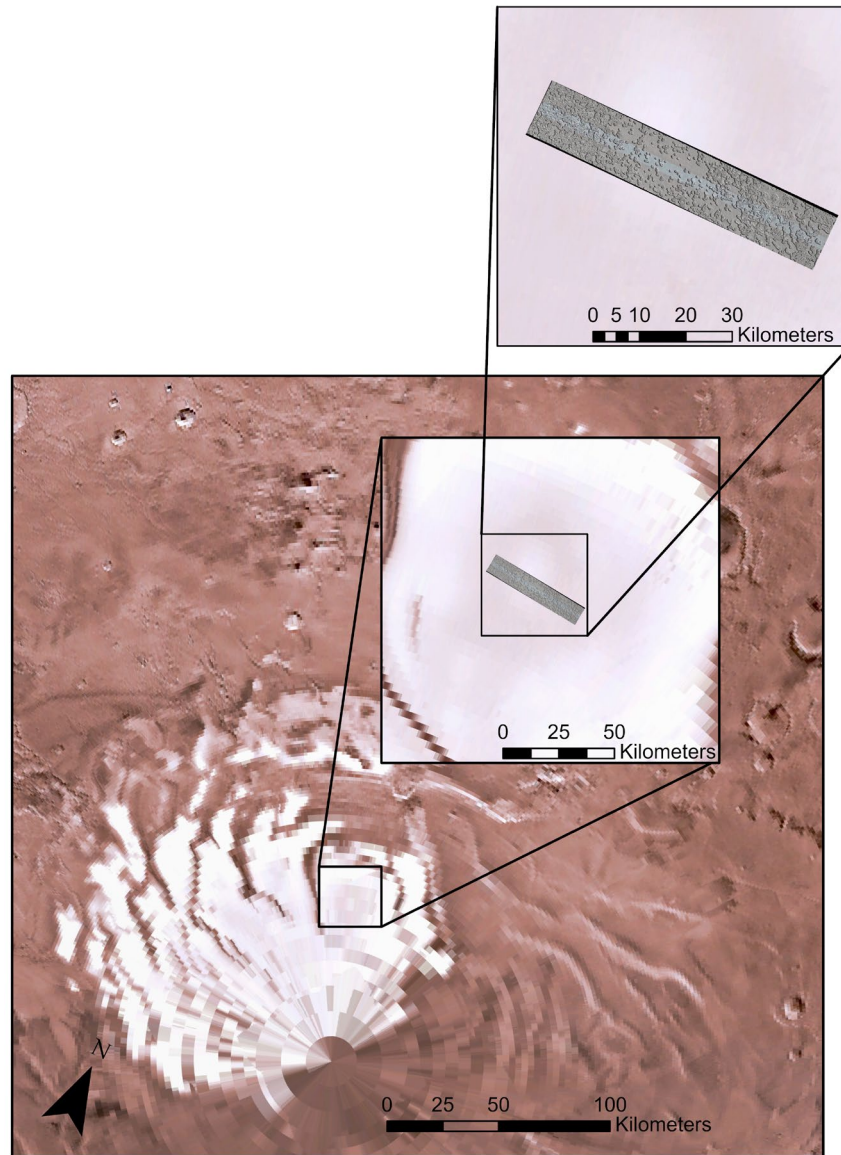


**Figure 1.** Full map of the Southern Pole of Mars including insets that show the size of the studied

images as compared to the size of the ice cap.

The Martian South Pole consists of four layers of ice; the top seasonal $CO_2$ cap, the residual water ice (Residual South Polar Cap), polar deposits consisting of water ice and dust, and finally the bottom Dorsa Argentea Formation. The Residual South Polar Cap (RSPC) is located at Planum Australe and is the host to the sublimation pits (Thomas et al., 2009; Figure 1). The average depth of the pits has been deduced at ~8 m using shadow measurements (Thomas et al. 2000). Some of the layers have been measured ~2 m thick using a shadow approach (Thomas et al. 2005). However, the research does note that not all the layers are of the same thickness, and that the thickness varies per feature. They counted the number of layers by using a trusted shadow technique.

Thomas et al. (2005) notes that there are two main units of deposition time, the older layer is Unit A, and the younger is Unit B. The paper separates the Unit A depression features into three categories: circular, curled, and elongate. Unit A is the host to the sublimation pits investigated in this thesis. A key finding in the Thomas et al. (2005) paper is that the depressions are located on a slope that is lower than 0. 3°, while the average slope of the RSCP is 0. 5°, this narrowed the regions that the pits are found. They concluded from Mariner 9 data that the deposition of Unit B was around the year 1972. The layers have also been studied showing that erosion occurs predominately in the $CO_2$ rich layers (Malin et al. 2001). Malin et al. (2001) found that 100-150g/cm$^2$ of $CO_2$ frost is deposited at 80° S each winter and sublimated back to the atmosphere every warm season. Due to the extreme levels of the factors needed for the $H_2O$ ice to go through this process, it was concluded that the erosional degradation is strictly with the $CO_2$ ice. The RSPC, as found by Thomas et al. (2009), has a mass of roughly 380 km$^3$. That totals less than 3% of the total mass of the Martian atmosphere. The study of the Swiss Cheese Terrain helped date the ice

deposits by looking at the edge retreat of the features. The Thomas et al. (2009) paper also provides

modifications to the feature classification that was first set in his earlier paper in 2005.
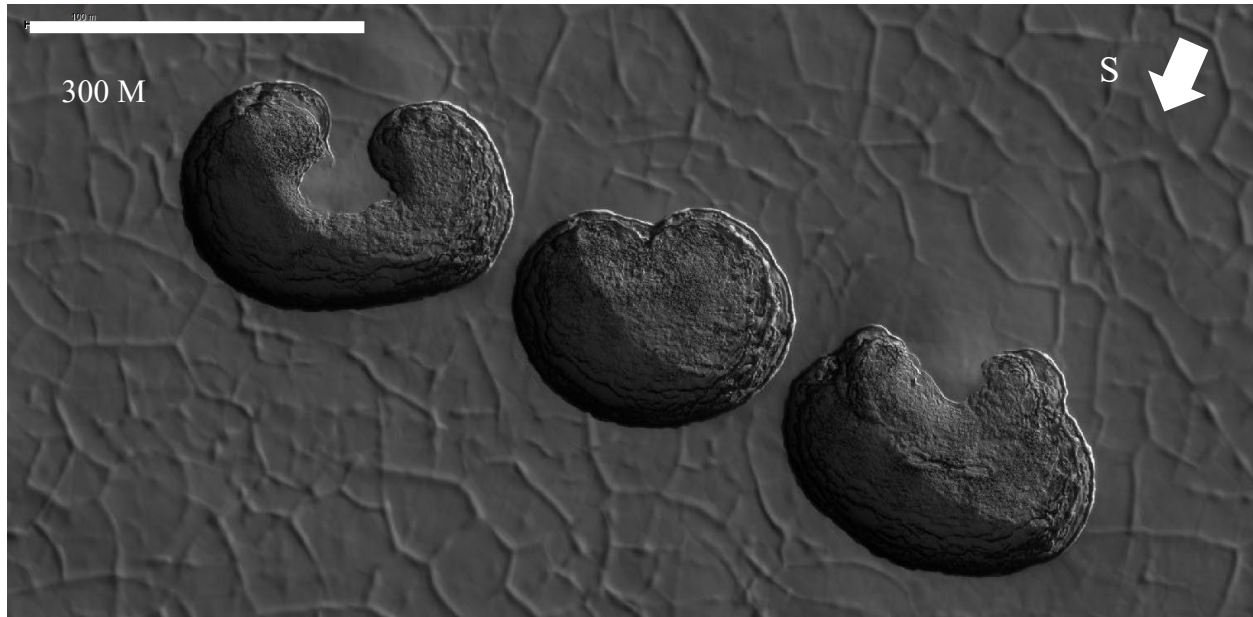


**Figure 2.** $CO_2$ sublimation pits, also known as Swiss Cheese Features, located on the Residual South Polar Cap (RSCP). A portion of HiRISE image ESP_023570_0930.

The sublimation features shown in Figure 1 are labeled as A1 units, however there are a few different shapes of the features. Unit A1 is larger than the similar unit of A0 and are more solitary than grouped features; this may be due to the young age of the depressions. In Thomas et al. (2000), a statement is made about the location of the pits, finding that the pits are primarily located in regions of residual summer $CO_2$ ice. This establishes the difference between the northern and southern poles. This paper also notes that geographic location affects the shapes of the depressions, the A1 units are located at a higher latitude than other unit types.

**Data and Methodology**

**Image Collection and Processing**

The images used in this research are collected via the High-Resolution Imaging Science Experiment, also known as HiRISE, onboard the Mars Reconnaissance Orbiter (MRO). HiRISE was designed to study the geological processes happening on the red planet by using a push-broom swath (figure 3) width of 6 kilometers and a length of up to 60 kilometers. Push-broom scanners are perpendicular to the flight path. The camera is able to collect longer frames of each pixel, as apposed to other types of image collection methods.
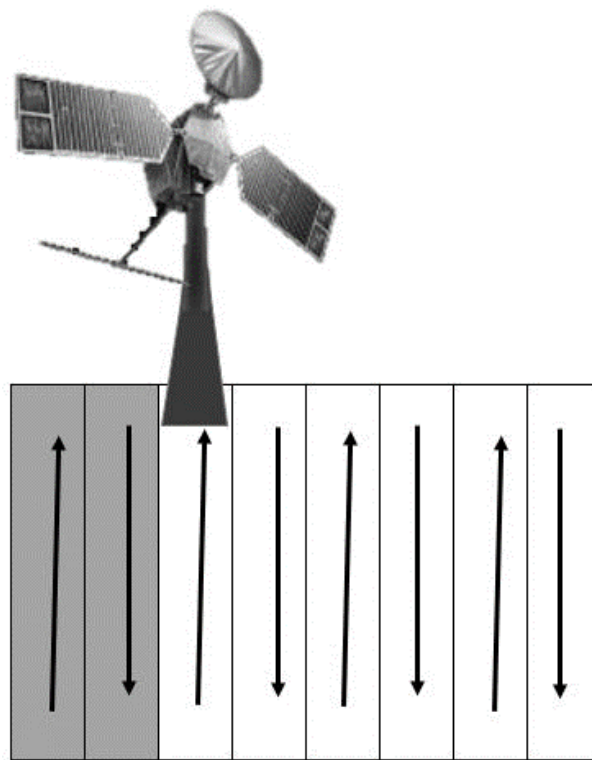


**Figure 3**. Illustration showing the HiRISE push-broom effect. This captures long cohesive images along a straight line.

The altitude varies from 200-400 kilometers above the surface and the images are taken using 3 main color filters. The filters are as follows: ten red bands are centered at a wavelength 0.694 μm, two blue-green bands centered at 0.536 μm, and two near-infrared bands centered at 0.874 μm (figure 4).
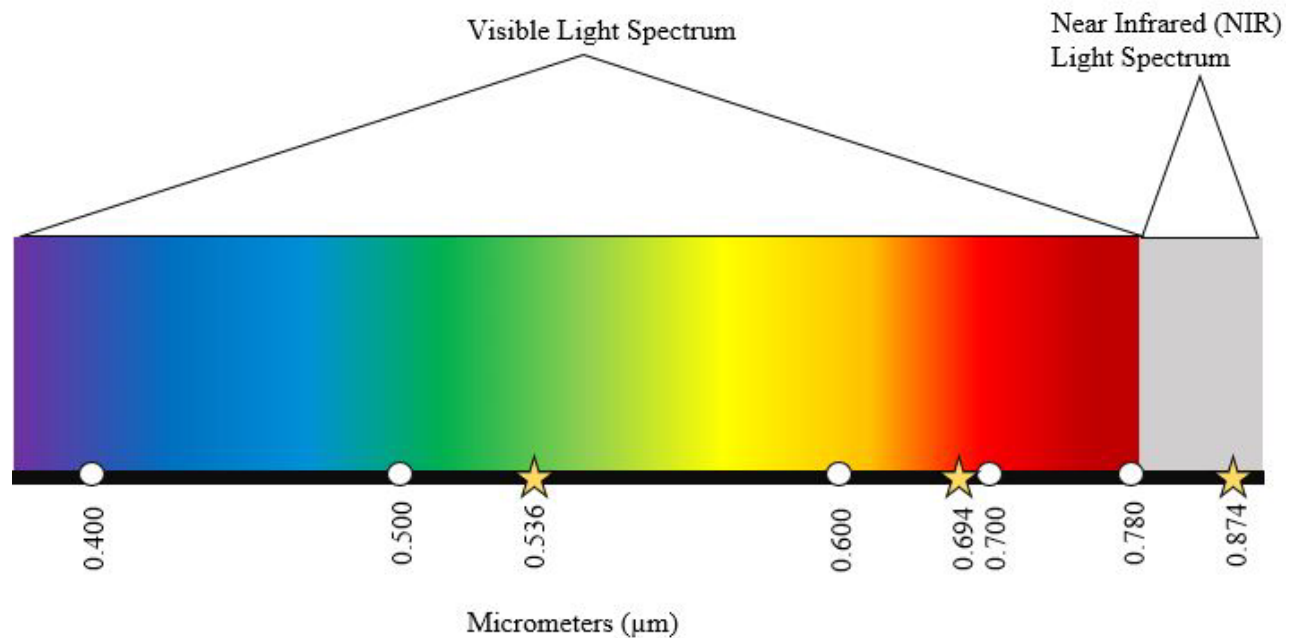


**Figure 4.** The visible and near infrared (NIR) light spectrum. The white circles represent the standard shifts, while the yellow stars represent the three filters collected through HiRISE.

The nominal spatial resolution has been described as 0.25 m/pixel. These images, once collected, are stored in the Mars Orbital Data Explorer section of the Planetary Data Science (PDS) Geoscience Node. These images are preprocessed for atmospheric corrections, areal distortions, and redundances before being stored in the PDS. HiRISE images can also be used to create Digital Elevation Models (DEMs). These can be used to further this research into a volume-based question rather than topical area.

**Object-Based Image Analysis**

OBIA increased in popularity in the late 1990's and early 2000's with the launch of several groups of satellites with visible color imaging technology. The processing of these images needed a higher-accuracy and more reliable automated or semi-automated remote sensing image processing techniques. Definiens Earth Sciences Business, an OBIA tool and algorithm software company, launched their software eCgonition in 2000. This product was the first of its kind (Blaschke 2010). OBIA was proven a success through processing of the initial release of the images from the satellite IKONOS. Fraser et. al (2002) created building models from the University of Melbourne. They used the IKONOS imagery in eCognition to gain information from the spectral, contextual, and DSM (digital surface model) derivations. A similar approach was researched by van der Sande et al. (2003) to model major flooding events in Itteren and Borgharen, Netherlands. They had success in land cover mapping, while further study was needed for residential areas and roads. This came about in Zhang & Couloigner (2005) when they were able to use a k-means clustering segmentation to identify and separate roads from parking lots in IKONOS imagery.

OBIA has also been applied in neural networking for medical imaging analysis. Yang and Yu (2021) introduce the multiple ways OBIA is used in the medical industry. They are simplified into two frameworks: one-stage and two-stage detections. For two stage detections, preprocessing and extracting the features of interest without categorization is the first step. The second step is to label the categories based on selected criteria. The one-step detection integrates both steps into one algorithm and was created due to the large data file restrictions on the two-step. While they recommend the use of OBIA in fields such as radiology, cardiovascular and digestive systems, they do note that the initial preprocessing requires substantial amount of already selected features.

**OBIA Ruleset Design**

The software Trimble eCognition v 9.1 is the vessel used to process the HiRISE images. This software was made available through collaboration with the University of Arkansas Center for Advanced Spatial Technologies (CAST). The images located in the RSPC were collected from the PDS Geoscience Node.

As a semi-automatic, hierarchical lineage approach to remote sensing techniques of processing, the OBIA approach used has six steps starting with segmentation (Figure 3). Segmentation is the process of sectioning the image into purposeful objects based on parameters such as homogeneity of spatial or spectral identifiers. A purposeful object is established when a desired object is selected based on the parameters used. For this study a purposeful object could be the non-pit mesa area, larger merged-pits, inner shadows, etc.
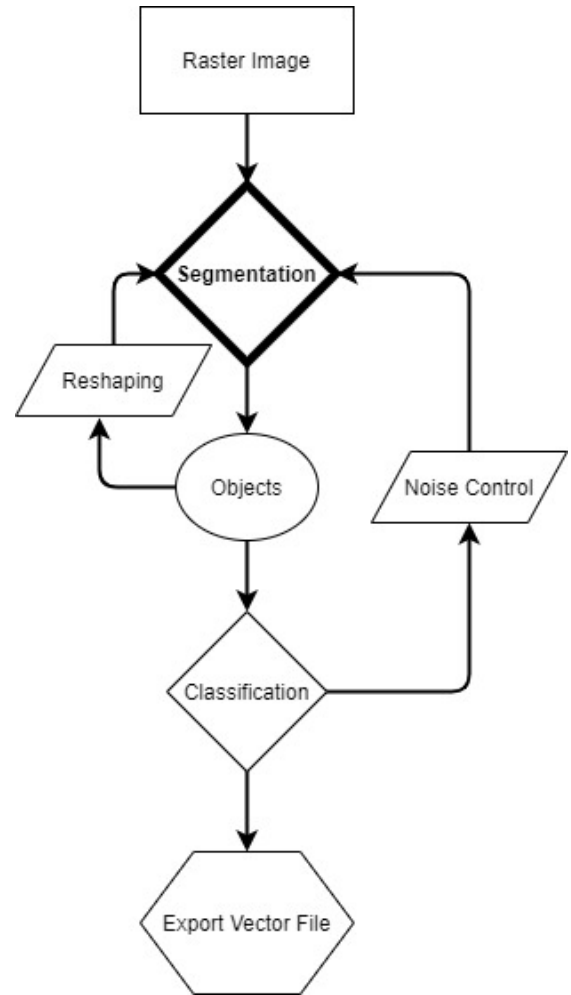


**Figure 5.** Image process step chart highlighting the first step of segmentation. This figure is representative of the ability of OBIA to be non-linear when re-shaping the target objects.

This first step is the Multiresolution Segmentation tool. This tool is located at the top of the "ruleset" and holds multiple variables such as shape, size, texture,

location, and several other options. Multiple variables can be used as a combination scale parameter in the ruleset, for example, polygonal shape recognition, the OBIA homogeneity value, and albedo minimum. This method allows for class hierarchy to systematically categorize the purposeful image objects into a multilevel format (e.g., circularity is a subcategory of homogeneity). For the purposed of this project, three classes were identified: pit, non-pit, and merged pit. These classes were determined based on the gray-level co-occurrence matrix (GLCM) homogeneity, pixel-brightness, shape, and size of segmented polygons.
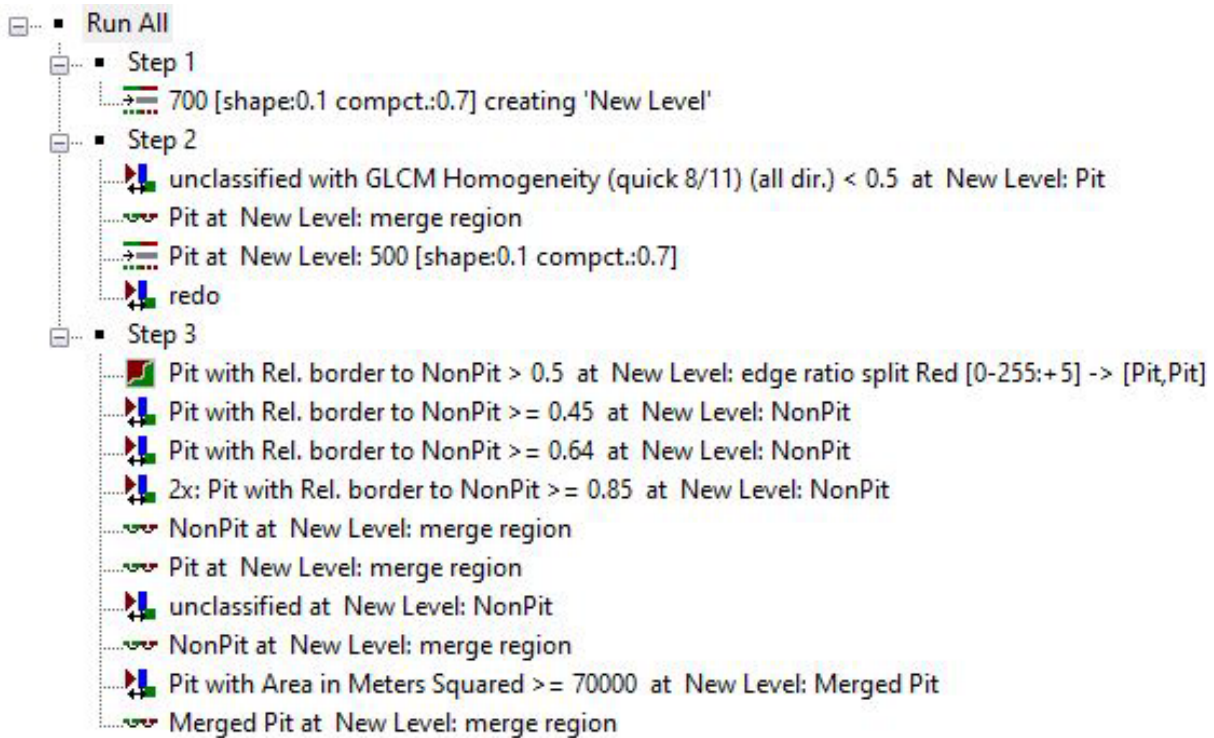


**Figure 6.** eCognition ruleset. Step one is the segmentation tool. Step two is the initial classification of $CO_2$ sublimation pits and merging those polygons into one feature class. Step Three is noise control and polygon border clean up, it also classifies the extra polygons.

Object reshaping is the next step in the process. This involved using contextual metrics such as nearest neighbor to refine the polygonal objects. Many other tools in the software are available to be used at differing times in the ruleset such as the merging of small, homogeneous objects into the larger surrounding objects based on relational border percentage, the breaking of larger objects into smaller objects, or even shrinking objects to meet parameter thresholds. After the objects were refined, objects were then classified into selected class titles. The combinations of variables were run and rerun in a subsegment of the ruleset to create a seamless and effective categorization that comes after the refinement stage. Categorizing these objects into the class of interest resulted in one cohesive export that includes all selected variables. This export is a .shp (Shapefile) that can be used for multiuser access and import into a geographic information system (GIS) software environment, in this case, ArcGIS Pro 2.

For each of the images, a difference set of values needed to be used for the differing scale parameters. This is due to zenith angle changes during the year and the varying times of the Martian year that the images were taken. These changing values are listed in table 1.

**Table 1.** A list of the parameter values in Step 1.

| Image | Scale Parameter | Shape | Compactness |
|---|---|---|---|
| psp_004687 | 700 | 0.1 | 0.7 |
| esp_014141 | 700 | 0.1 | 0.7 |
| esp_023570 | 700 | 0.1 | 0.7 |
| esp_038206 | 700 | 0.1 | 0.7 |

| Image | | | |
|---|---|---|---|
| esp_041094 | 700 | 0.1 | 0.7 |
| esp_047661 | 700 | 0.1 | 0.7 |

**Table 2.** A list of the parameter values in Step 2.

| Image | Homogeneity | Scale Parameter | Shape | Compactness |
|---|---|---|---|---|
| psp_004687 | 0.2 | N/A | N/A | N/A |
| esp_014141 | 0.31 | N/A | N/A | N/A |
| esp_023570 | 0.45 | 150 | 0.1 | 0.7 |
| esp_038206 | 0.42 | 100 | 0.1 | 0.7 |
| esp_041094 | 0.3 | 250 | 0.1 | 0.7 |
| esp_047661 | 0.46 | 100 | 0.1 | 0.7 |

**Table 3.** A list of the parameter values in Step 3.

| Image | Merge Rel. Border | Assign Class Rel. Border | Assign Class Rel. Border | 2x Assign Class Rel. Border | Assign Class Area |
|---|---|---|---|---|---|
| psp_004687 | N/A | N/A | N/A | N/A | N/A |

| | | | | | |
|---|---|---|---|---|---|
| esp_014141 | N/A | N/A | N/A | N/A | N/A |
| esp_023570 | 0.5 | 0.45 | 0.64 | 0.85 | 70,000 |
| esp_038206 | 0.5 | 0.45 | 0.64 | 0.85 | 70,000 |
| esp_041094 | 0.5 | 0.45 | 0.64 | 0.85 | 70,000 |
| esp_047661 | 0.5 | 0.95 | 0.5 | 0.85 | 70,000 |

**Geographic Information Systems**

Geographic information systems (GIS) is the integration of compiling, manipulating, and analysis of spatial data. This system lets the user see the metadata of a map by applying the geographic attributes of the specified region to a computer-based system for evaluation as a function of a physical map. Early work of GIS began in the 1850's by Dr. John Snow. Survey based mapping techniques were used to trace the source of a cholera outbreak in London, United Kingdom (Snow 1855). Until the 1960's, GIS was hand drawn maps with hand-measured survey's techniques like Dr. Snow's work. Roger Tomlinson of Canada created the first computerized GIS system, on behalf of the Canadian government for land-use management (Dangermond 2014).

Environmental Systems Research Institute, Inc (Esri) was founded in 1969 and quickly became the forerunner for a GIS computerized software company. Originally created to help with land use and management planning, Esri developed an abundance of spatial analysis tools and methods to be utilized by a wide range of end-users. The first Arc product was released in 1981,

and in 2015 ArcGIS Pro v. 1.0 was released for a more end-user interface and even more tools to complete additional analyses.

**Geospatial Analysis**

The software Esri ArcGIS Pro (ArcPro) v. 2.9 was selected for the purposed of this study. This software was made available through collaboration with CAST. The exported data from eCognition was fed into ArcGIS Pro as layers (Figure 5) and added into a file geodatabase. A geodatabase (GDB) is the collection of all layers and metadata into a composite structure. The layers in the GDB overlay one another in a manner similar to stacking paper. The characteristics of each layer are totaled together onto one layer for a complete analysis. This is necessary for two reasons, the first is the size of the file is lowered. With fewer layers, the file size and run time for any further tools are shorter. The second reason is to support the overall statistical analysis. Each layer includes the area in meters squared.
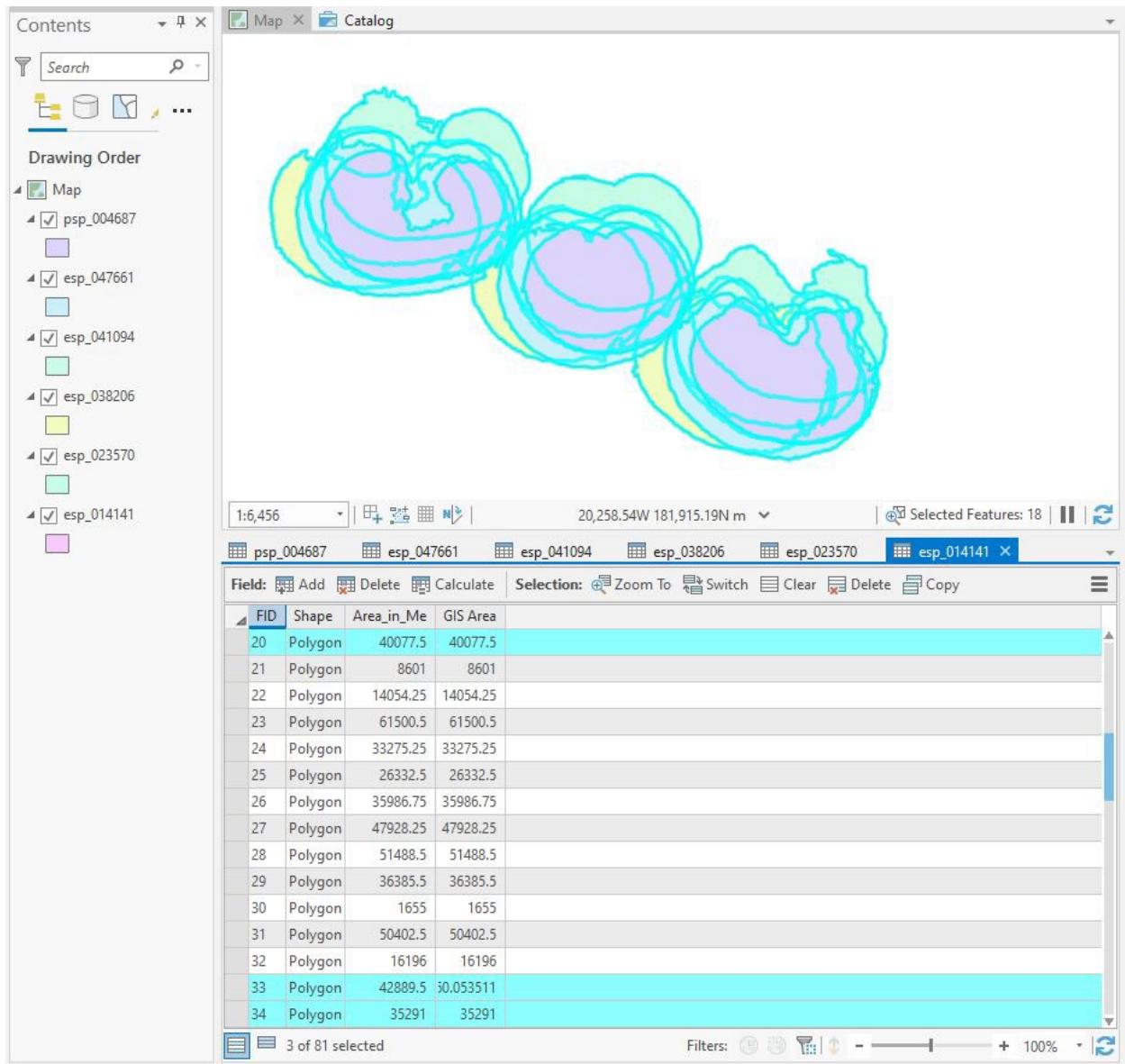
**Figure 7.** This graphic shows the overlayed polygons in ArcGIS Pro from the eCognition exported files. It also shows the area for the three pits in the esp_014141 image. Please see Table 2 for image reference.

**Verifiability**

An accuracy assessment was done to compare the semi-automated process to a hand calculated measurement. The initial image used was portioned down from the complete ESP_023570_0930 HiRISE image acquired on August 7, 2011. The hand-picked ruleset identified the three varieties of sublimation pits in this image portion and simultaneously measured their area. Prior to displaying the extrapolated geodatabase in ArcGIS, pit polygons were manually digitized. Digitizing is defined as when the manual user selects vertices to form polygons around the target objects and add them to a geodatabase. These polygon layers are overlaid on top of each other and the number of pixels in the polygon was tabulated (Table 1). This was done as a verification system against the OBIA ruleset. In each step of the OBIA ruleset, each letter corresponds to the next portion of the hierarchical segmentation process. Scale and orientation are reflected (Figure 6): A) displays the results from the segmentation portion of the ruleset, B) exhibits the outcomes from the classification section, C) is the product of merging the segmented classes together, and D) reveals how morphology can clean up the edges and bring the shape of the shape of the polygon to the shape of the sublimation pit.
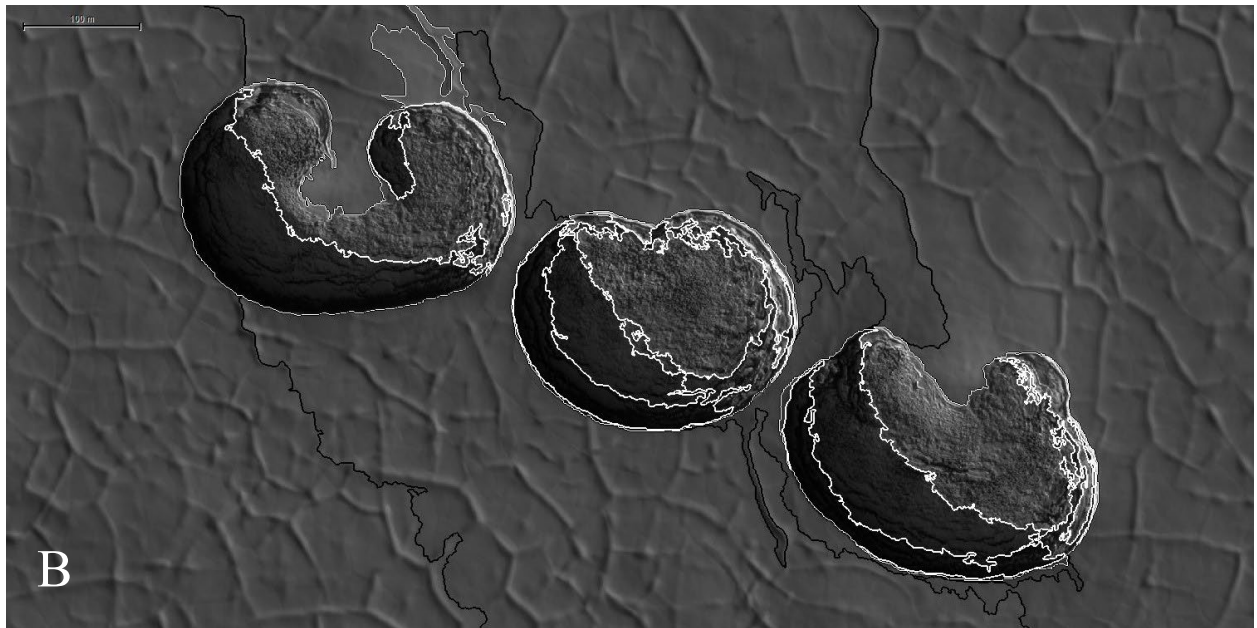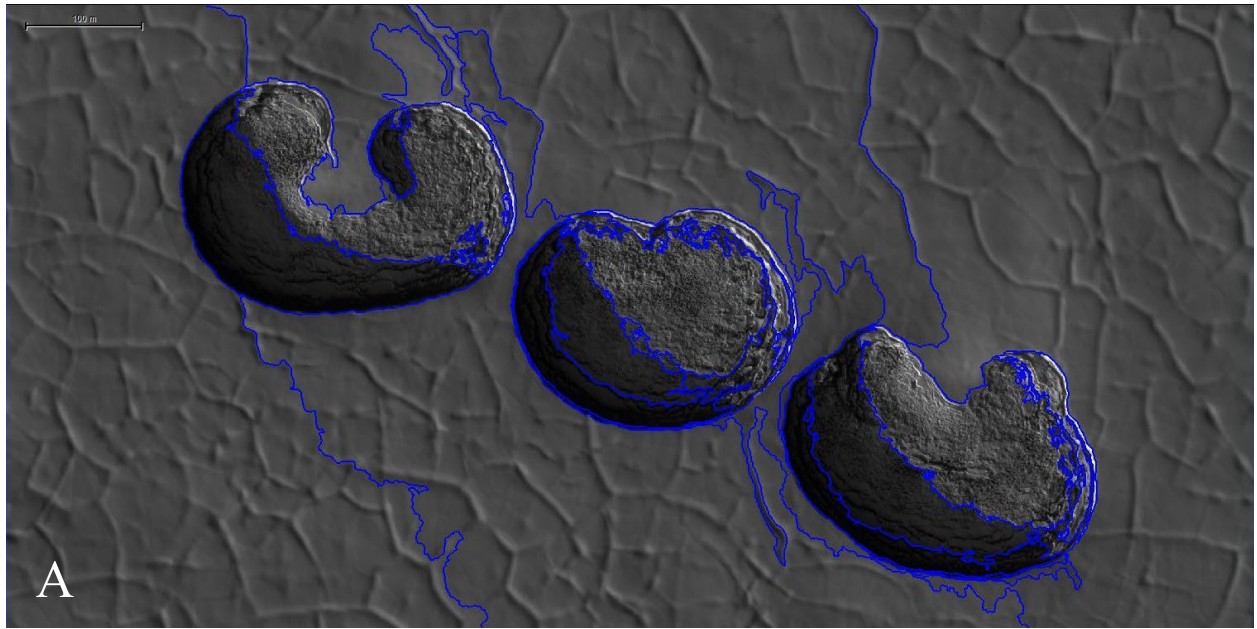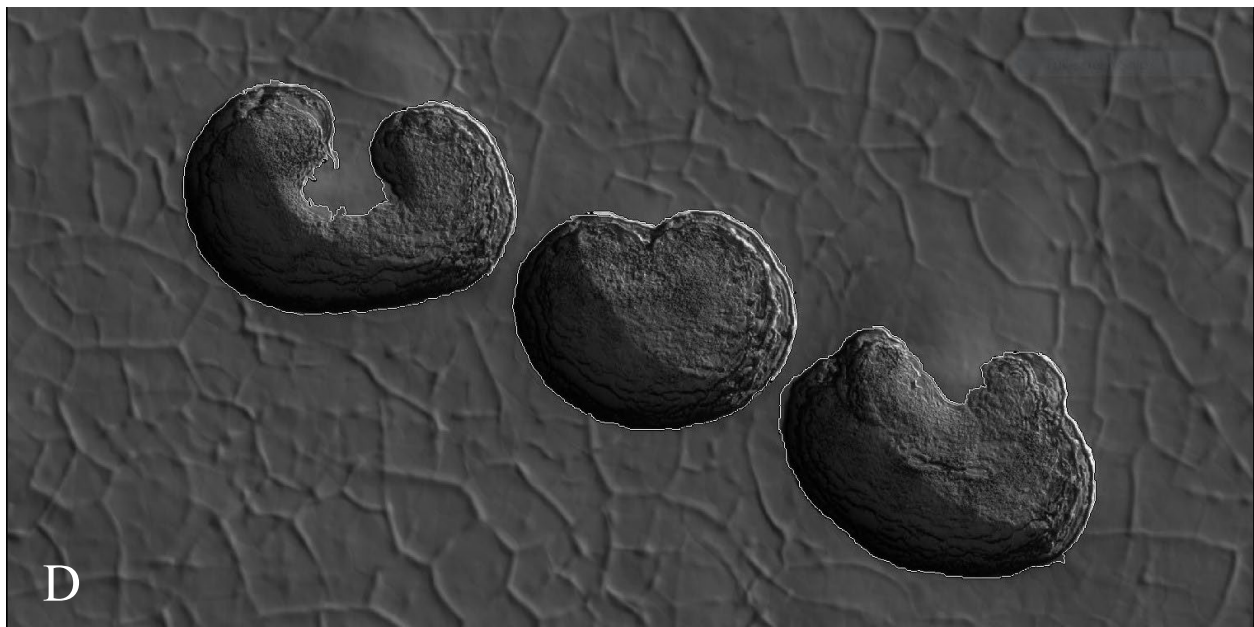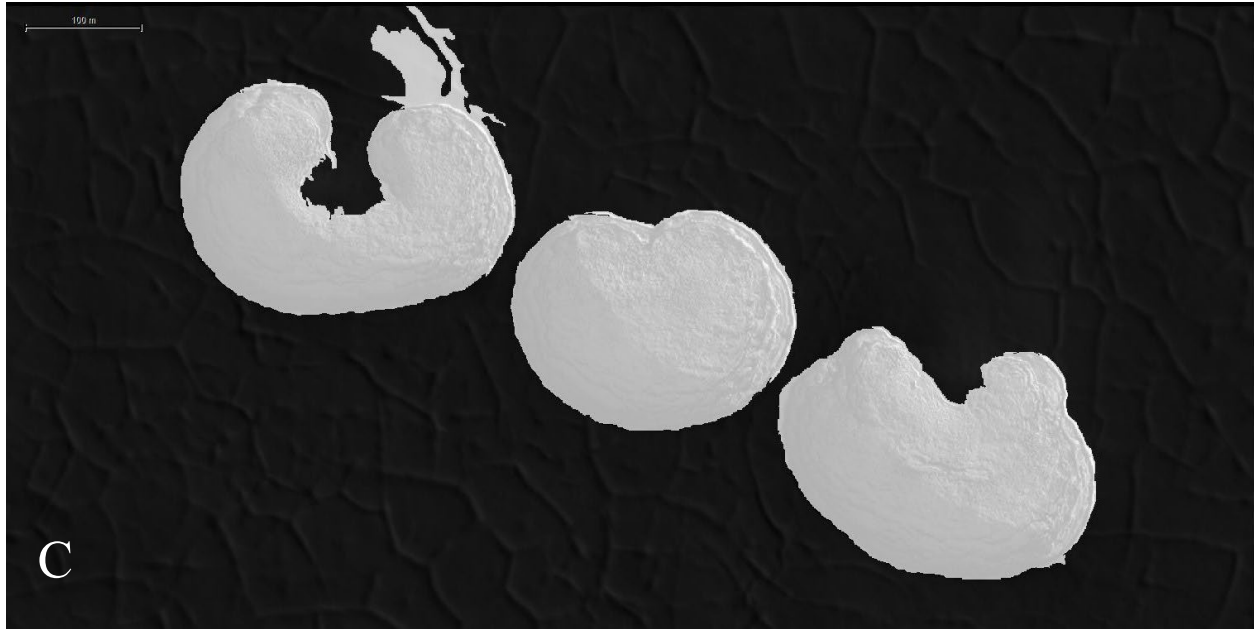
**Figure 8.** Each step of the ruleset. A) Segmentation B) Classification C) Feature Class Merge D) Noise Control. The outline of each polygon is a light gray.

**Table 4.** This table displays the calculated areas of each sublimation pit with the OBIA, and the

hand digitized in ArcMap in meters squared.

| Pit Area in Meters Squared | | | |
|---|---|---|---|
| Pit | OBIA | Hand | % Diff. |
| Left | 41798 | 41388 | 0.9809 |
| Center | 37582 | 37492 | 0.2395 |
| Right | 43228 | 42796 | 0.9994 |
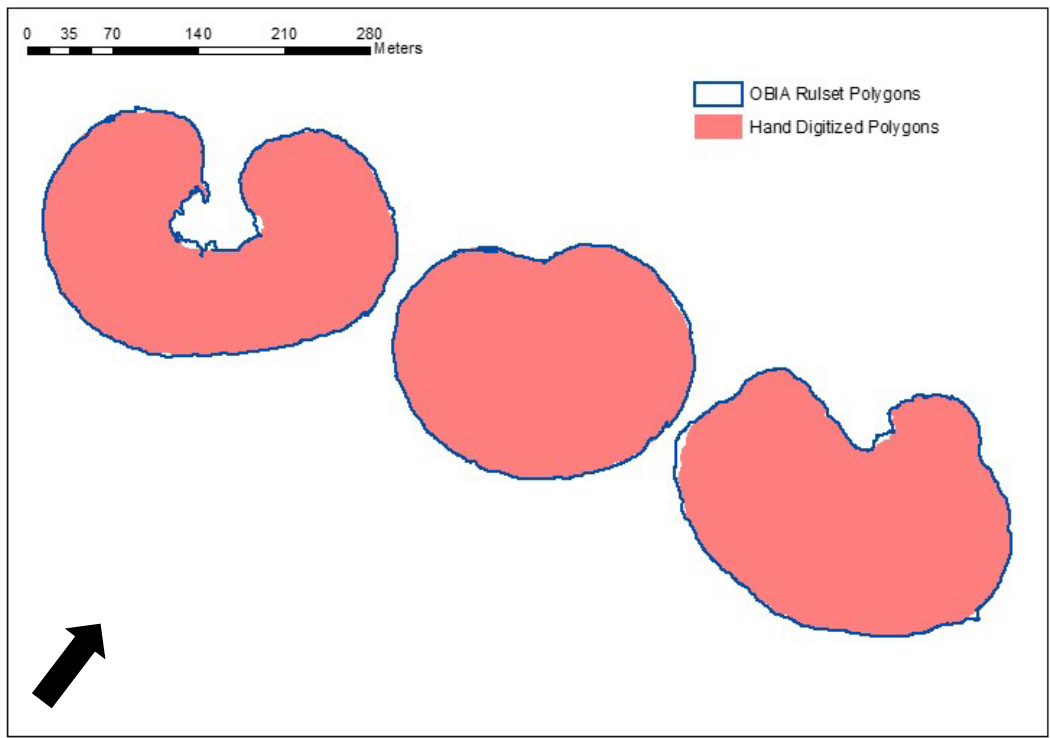


**Figure 9.** An image of the final product of the two polygon shapefiles. The OBIA ruleset is the

blue line, and the hand digitized polygons are symbolized in red.

The simultaneous measurement of the three selected sublimation pits was successful. The

left pit has an area difference of approximately 410 $m^2$ between the OBIA polygon and the

digitized polygon, the center pit has a ~90 m$^2$ area difference, and the right pit has a ~432 m$^2$ area difference (Swick et al. 2020). Compared to manual measurements done in ArcGIS, eCognition separated by less than a 1% margin of difference (Table 1). This small margin can be attributed to human error or precision of OBIA (or both). The success of the preliminary result led to a positive outlook toward the remainder work of this study discussed in the following section.

**Results and Discussion**

OBIA versus pixel-based image analysis has been performed on several occasions for Earth-based science research. In 2003, Yan compared object-oriented image analysis done through eCogntion to pixel-based image analysis by researching Chinese coal fires. By using ASTER and Landsat images, Yan cross classified the exported objects and concluded that object-oriented analysis gave a "more reasonable" success rate (Yan 2003). They stated limitations would include land change over time that could provide inaccuracies if the research were to be replicated. In another form, object-orientated analysis was used to restore legacy population data that was originally processed by pixel-based assessments (Kerle & Leeuw 2009).

Reproducibility and replicability (R&R) are defined separately by the National Academy of Sciences (Committee on Reproducibility and Replicability in Science 2019). Reproducibility in research gives access to all available data for the research findings to be checked. Replicability differs in that different data and/or methods are used to address the same question. Both require that the results be the same as the original conclusion. The data used in this research were collected from the Mars Orbital Data Explorer repository of the NASA Planetary Data System Geoscience Node, also known as the PDS Geosciences Node Mars ODE. The images are downloaded as a .jp2 version type. All images come with metadata listing the processing and handling of the images

from the PDS node. The images also come with the information of the radiometric correction procedures and reference documents. Once the images were downloaded, and in support of R&R, all images and data processed there-after were then uploaded into a dedicated open access archive using the Center for Open Science Open Science Framework. In addition to this repository, the data is also stored in the Center for Advanced Spatial Technologies (CAST) storage area network.

The results of the object-based image analysis on the three Martian sublimation pits are outlined in this section. The ruleset utilized in the preliminary work was used as the baseline for creating the processes for the additional images. Following the success of the initial image, an addition 5 images were processed with eCognition. Some modifications had to be done to account for the zenith angle changes in the various images. The .shp file exports were then placed into ArcGIS Pro where the specified polygons were remeasured for accuracy. The surface level area was taken and analyzed for the expansion per Earth (EY) and Martian (MY) year.

Six additional images were analyzed and are listed in Table 2. Due to the images being taken at different times of the Martian day and seasonal changes, the SPs for polygon sizes needed to be adjusted, as well as the color parameters. The color parameters needed to be changed due to adding in images with darker shadows and more reflective areas due to the zenith angle.

**Table 5.** A list of the six HiRISE images analyzed, and the Earth and Martian year that these were taken.

| Earth Year | Mars Year | Image |
|---|---|---|
| 2007 | 27 | psp_004687 |
| 2009 | 29 | esp_014141 |
| 2011 | 30 | esp_023570 |
| 2014 | 32 | esp_038206 |
| 2015 | 32 | esp_041094 |
| 2016 | 33 | esp_047661 |

With these image-objects it was found that the pits increase linearly over 5 Martian years (MY) and 9 Earth years' (EY) time. The three pits used for this project show evidence of stable growth over time with a small outlier happening in 2007 with the right pit (Figure 8). The nearly linear growth shown in the dotted trend lines (Figure 8) indicates that the $CO_2$ is being sublimated at a higher rate than the amount of $CO_2$ being retained each winter. The atmosphere at the poles condenses into the seasonal caps, while the rest of the caps are controlled by the global Hadley cells. The Hadley cells are what drives the Martian atmosphere and are inverted between the seasons (Keiffer et al. 1979). By taking the growth of each image and the yearly progression, this work has established a growth rate of approximately 1,608 $m^2$/EY for the left pit, ~919 $m^2$/EY for the center pit, and ~942 $m^2$/EY for the right pit (Cleveland et al. 2022). By dividing these rates by

1.88 to account for the EY to MY change, the result is approximately ~855 m$^2$/MY for the left pit, ~489 m$^2$/MY for the center pit, and ~501 m$^2$/MY for the right pit. By taking the average growth rate and using the final area estimates, it was found that the left pit is roughly 62 MY old, the center pit is ~87 MY old, and the right pit is ~97 MY old.
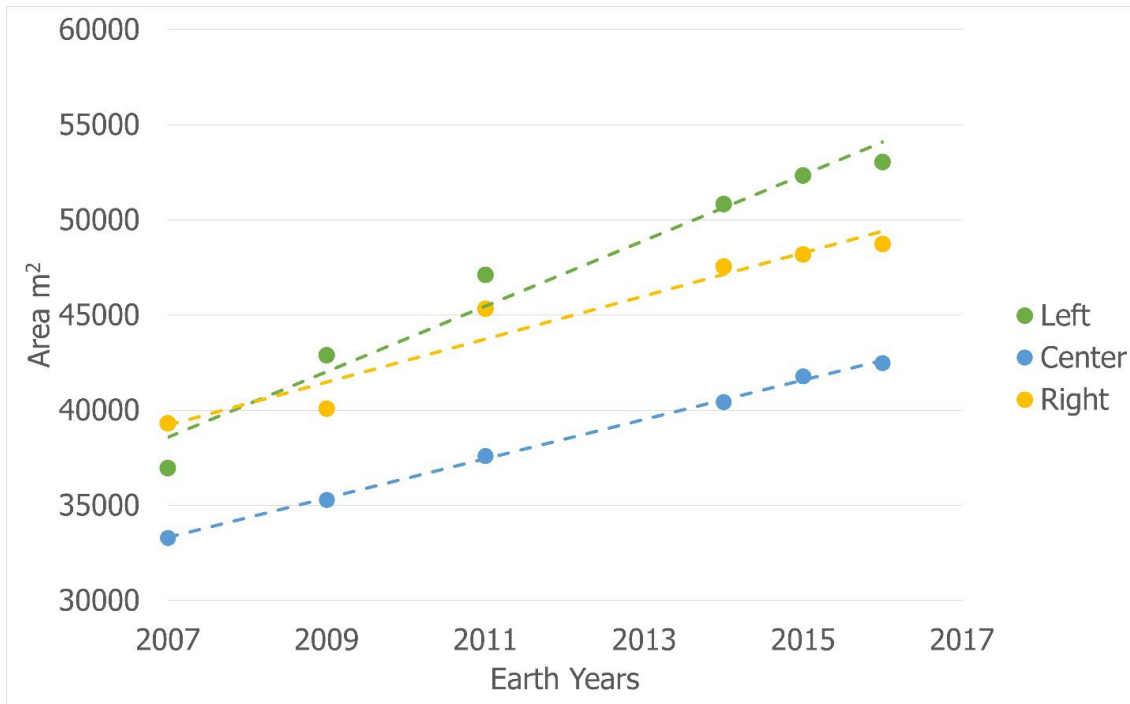


**Figure 10.** Surface area of the investigated three pits (Figure 1) as a function of time in Earth years.

These results correlate with the model created by Byrne 2003, which found an initial feature creation aging around 1600-1920 EY. They found a most likely start range is around ~1900 EY, while our measurements deduce a range of ~1830-1900 with an average start year of ~1862 EY.
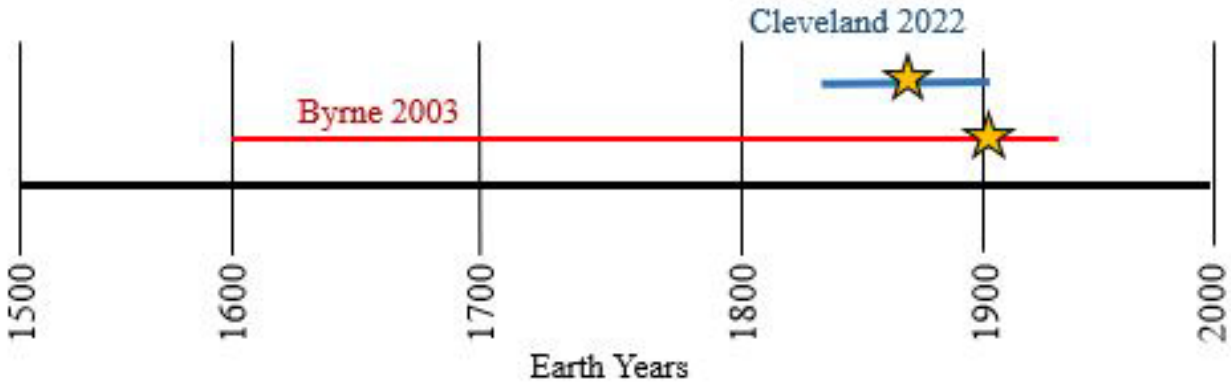
**Figure 11.** Timeline of starting ranges from both Cleveland 2022 and Byrne 2003. The yellow stars indicate where the average start year is for the data.

This measurement was calculated by the following equation:

$$Creation\ Earth\ Year = 2016 - \frac{MY\ old * 687}{365}$$

2016 is used as the date of retraction since that is the date of the most recent image used in this study. The Martian age of the pit multiplied by 687. 687 is the number of Earth days to one Martian year. The product of this is then divided by the number of days in an Earth year. The quotient of this is then subtracted from 2016. This calculation does not include leap year, which would add anywhere from 29-46 Earth days to the total if we were calculating this time in months or even days. However, this would only be an estimation and does not provide factual proof of an exact start date.

The slight difference in the estimated start year could be due to a variety of differences, such as spatial resolution. Byrne utilized THEMIS data which has a spatial resolution of ~100 m/pixel, while this investigation used HiRISE images which have a spatial resolution of ~0.25 m/pixel. We also have to consider the amount of data used. This research covers a time length of

26

nine Earth years, where Byrne does not list the time frame of data. There is a lack of research on the growth of the features. The current literature classifies the different types of topography on the poles. The lack of research could be due to the short geological timeline of the features. While the majority of geological features are studied on scales of thousands of years amid large climate changes, the Mars features under investigation change on a much shorter scale, that of hundreds of years.

**Conclusion**

This thesis project investigated the ability of the object-based image analysis (OBIA) technique to successfully accelerate the study of the Swiss Cheese Features (SCF) found on the Residual South Polar Cap (RSPC) of Mars. The object identification of SCF on the southern cap of Mars was found through creating an identification method during the processing of HiRISE images. The semi-automated processing used Trimble eCogntion software while the initial manual identification utilized Esri's ArcGIS Pro. ArcGIS Pro was also utilized in the measurement investigation of the multiple post-processed polygons. The process, while used widely in Earth science, has infrequently been applied in planetary science. The successful results of this study have proven OBIA can be used to be accelerate image-object processes for planetary images. With this study it was found that these features are no older than 100 Martian years of age, with the likely creation at Earth year ~1862.

# References

Blaschke, T. "Object Based Image Analysis for Remote Sensing." ISPRS Journal of

    Photogrammetry and Remote Sensing 65, no. 1 (January 2010): 2–16.

    https://doi.org/10.1016/j.isprsjprs.2009.06.004.

Byrne, S. "A Sublimation Model for Martian South Polar Ice Features." Science 299, no. 5609

    (February 14, 2003): 1051–53. https://doi.org/10.1126/science.1080148.

Chevrier, V F, M S Fusco, K Farnsworth, J P Knightly, and A Yazdani. "Time Evolution of

    Swiss Cheese Terrains in the Martian South Polar Cap," June 19, 2018, 2.

Cleveland, Racine, V. F. Chevrier, and J. A. Tullis. "AN OBJECT-BASED IMAGE ANALYSIS

    OF THE SWISS CHEESE TERRAIN EVOLUTION ON THE MARTIAN SOUTH

    POLE.2580.Pdf," 2022. https://www.hou.usra.edu/meetings/lpsc2022/pdf/2580.pdf.

Colwell, Robert N. "The Extraction of Data from Aerial Photographs by Human and Mechanical

    Means." Photogrammetria 20, no. 6 (December 1, 1965): 211–28.

    https://doi.org/10.1016/0031-8663(65)90013-X.

Committee on Reproducibility and Replicability in Science, Board on Behavioral, Cognitive, and

    Sensory Sciences, Committee on National Statistics, Division of Behavioral and Social

    Sciences and Education, Nuclear and Radiation Studies Board, Division on Earth and Life

    Studies, Board on Mathematical Sciences and Analytics, et al. Reproducibility and

    Replicability in Science. Washington, D.C.: National Academies Press, 2019.

    https://doi.org/10.17226/25303.

Conglaton, Russell. "Assessing Positional and Thematic Accuracies of Maps Generated from Remotely Sensed Data." In Remotely Sensed Data Characterization, Classification, and Accuracies, 583–601, 2016.

Dangermond, Jack. "Roger Tomlinson, Geographer." Esri (blog), November 14, 2018. https://www.esri.com/about/newsroom/arcnews/roger-tomlinson-geographer/.

Emran, Al, Luke J Marzen, and David T King Jr. "Automated Object-Based Identification of Dunes at Hargraves Crater, Mars," 1, n.d.

Fraser, C. S, E Baltsavias, and A Gruen. "Processing of Ikonos Imagery for Submetre 3D Positioning and Building Extraction." ISPRS Journal of Photogrammetry and Remote Sensing 56, no. 3 (April 1, 2002): 177–94. https://doi.org/10.1016/S0924-2716(02)00045-X.

Fusco, M S. "SPATIAL AND GEOMORPHOLOGICAL EVOLUTION OF SWISS CHEESE TERRAINS IN THE MARTIAN SOUTH POLAR CAP.," 2018. https://www.hou.usra.edu/meetings/lpsc2018/pdf/2682.pdf.

"HiRISE | High Resolution Imaging Science Experiment." Accessed January 25, 2022. https://www.uahirise.org/.

Im, J., J. R. Jensen, and J. A. Tullis. "Object-based Change Detection Using Correlation Image Analysis and Image Segmentation." International Journal of Remote Sensing 29, no. 2 (January 1, 2008): 399–423. https://doi.org/10.1080/01431160601075582.

Kass, D. M., A. Kleinböhl, D. J. McCleese, J. T. Schofield, and M. D. Smith. "Interannual Similarity in the Martian Atmosphere during the Dust Storm Season: DUST SEASON

INTERANNUAL SIMILARITIES." Geophysical Research Letters 43, no. 12 (June 28, 2016): 6111–18. https://doi.org/10.1002/2016GL068978.

Kerle, Norman, and Jan de Leeuw. "Reviving Legacy Population Maps With Object-Oriented Image Processing Techniques." IEEE Transactions on Geoscience and Remote Sensing 47, no. 7 (July 2009): 2392–2402. https://doi.org/10.1109/TGRS.2008.2010853.

Kieffer, Hugh H. "Mars South Polar Spring and Summer Temperatures: A Residual CO2 Frost." Journal of Geophysical Research: Solid Earth 84, no. B14 (1979): 8263–88. https://doi.org/10.1029/JB084iB14p08263.

Kleinböhl, A, D M Kass, S Piqueux, P O Hayne, and K Noguchi. "INTERHEMISPHERIC DIFFERENCES IN CO2 SUPERSATURATION AND CO2 GAS DEPLETION IN MARS' POLAR WINTER ATMOSPHERE FROM MARS CLIMATE SOUNDER OBSERVATIONS.," no. 2099 (2020): 2.

Knightly, Paul. "Temporal Variations of Swiss Cheese Terrain - NASA/ADS," 2019. https://ui.adsabs.harvard.edu/abs/2019LPI....50.2187K/abstract.

Malin, M. C. "Observational Evidence for an Active Surface Reservoir of Solid Carbon Dioxide on Mars." Science 294, no. 5549 (December 7, 2001): 2146–48. https://doi.org/10.1126/science.1066416.

mars.nasa.gov. "HiRISE." Accessed May 22, 2022. https://mars.nasa.gov/mro/mission/instruments/hirise/.

McEwen, Alfred S., Eric M. Eliason, James W. Bergstrom, Nathan T. Bridges, Candice J. Hansen, W. Alan Delamere, John A. Grant, et al. "Mars Reconnaissance Orbiter's High

Resolution Imaging Science Experiment (HiRISE)." Journal of Geophysical Research 112, no. E5 (May 17, 2007): E05S02. https://doi.org/10.1029/2005JE002605.

MEPAG Goals Committee. "Mars Science Goals, Objectives, Investigations, and Priorities: 2020 Version," 2020, 86.

AGU Newsroom. "Multiple Former Ice Caps Buried under Mars's North Polar Ice." Accessed May 22, 2022. https://news.agu.org/press-release/multiple-former-ice-caps-buried-under-marss-north-polar-ice/.

Neumann, Gregory A., David E. Smith, and Maria T. Zuber. "Two Mars Years of Clouds Detected by the Mars Orbiter Laser Altimeter." Journal of Geophysical Research: Planets 108, no. E4 (2003). https://doi.org/10.1029/2002JE001849.

Pedersen, Gro B M, and Pablo Grosse. "TOPOGRAPHIC FINGERPRINT OF ERUPTION ENVIRONMENT: EVIDENCE FROM REYKJANES," 2013, 2.

Sande, C. J. van der, S. M. de Jong, and A. P. J. de Roo. "A Segmentation and Classification Approach of IKONOS-2 Imagery for Land Cover Mapping to Assist Flood Risk and Flood Damage Assessment." International Journal of Applied Earth Observation and Geoinformation 4, no. 3 (June 1, 2003): 217–29. https://doi.org/10.1016/S0303-2434(03)00003-5.

Sholes, S F, V F Chevrier, and J A Tullis. "Object Based Image Analysis for Remote Sensing of Planetary Surfaces.," 2013, 2.

Snow, John. On the Mode of Communication of Cholera. London : John Churchill, 1855. http://archive.org/details/b28985266.

Swick, Racine, V. F. Chevrier, and J. A. Tullis. "AN OBJECT-BASED IMAGE ANALYSIS OF

THE SWISS CHEESE TERRAIN EVOLUTION ON THE MARTIAN SOUTH POLE:

PRELIMINARY RESULTS.," 2020.

https://www.hou.usra.edu/meetings/lpsc2020/pdf/2628.pdf.

Thomas, P. C., M. C. Malin, K. S. Edgett, M. H. Carr, W. K. Hartmann, A. P. Ingersoll, P. B.

James, L. A. Soderblom, J. Veverka, and R. Sullivan. "North–South Geological

Differences between the Residual Polar Caps on Mars." Nature 404, no. 6774 (March

2000): 161–64. https://doi.org/10.1038/35004528.

Thomas, P.C., P.B. James, W.M. Calvin, R. Haberle, and M.C. Malin. "Residual South Polar

Cap of Mars: Stratigraphy, History, and Implications of Recent Changes." Icarus 203, no. 2

(October 2009): 352–75. https://doi.org/10.1016/j.icarus.2009.05.014.

Thomas, P.C., M.C. Malin, P.B. James, B.A. Cantor, R.M.E. Williams, and P. Gierasch. "South

Polar Residual Cap of Mars: Features, Stratigraphy, and Changes." Icarus 174, no. 2 (April

2005): 535–59. https://doi.org/10.1016/j.icarus.2004.07.028.

Vamshi, Gasiganti T., Tapas R. Martha, and K. Vinod Kumar. "An Object-Based Classification

Method for Automatic Detection of Lunar Impact Craters from Topographic Data."

Advances in Space Research 57, no. 9 (May 2016): 1978–88.

https://doi.org/10.1016/j.asr.2016.01.022.

Yan, Gao. "Pixel Based and Object Oriented Image Analysis for Coal Fire Research."

international institute for geo-information science and earth observation enschede, the

netherlands, 2003.

https://webapps.itc.utwente.nl/librarywww/papers_2003/msc/ereg/gao_yan.pdf.

Yang, Ruixin, and Yingyan Yu. "Artificial Convolutional Neural Network in Object Detection and Semantic Segmentation for Medical Imaging Analysis." Frontiers in Oncology 11 (2021). https://www.frontiersin.org/article/10.3389/fonc.2021.638182.